Supramolecular Peptoid Structure Strengthens Complexation with Polyacrylic Acid Microgels

Wenhan Zhao,[1] Jennifer S. Lin,[2] Josefine Eilsø Nielsen,[2,3] Kristian Sørensen,[2] Anand Sunil Wadurkar,[4] Jingjing Ji,[4] Annelise E. Barron,[2] Shikha Nangia[4] and Matthew R. Libera[1*]

[1] Department of Chemical Engineering and Materials Science
Stevens Institute of Technology, Hoboken, NJ, 07030 United States

[2] Department of Bioengineering, School of Medicine & School of Engineering,
Stanford University, Stanford, CA, 94305 United States

[3] Department of Science and Environment, Roskilde University, Roskilde, DK-4000 Denmark

[4] Department of Biomedical and Chemical Engineering,
Syracuse University, Syracuse, NY, 13244 United States

[*] mlibera@stevens.edu
contact author

Keywords: complexation, peptoids, supramolecular, antimicrobial, microgel, self-assembly

Abstract:

We have been studying the complexation between cationic antimicrobials and polyanionic microgels to create self-defensive surfaces that responsively resist bacterial colonization. An essential property is the stable sequestration of the loaded (complexed) antimicrobial within the microgel under physiological ionic strength. Here we assess the complexation strength between poly(acrylic acid) [PAA] microgels and a series of cationic peptoids that display supramolecular structures ranging from an oligomeric monomer to a tetramer. We follow changes in loaded microgel diameter with increasing [Na^+] as a measure of the counterion doping level. Consistent with prior findings on colistin/PAA complexation, we find that a monomeric peptoid is fully released at ionic strengths well below physiological conditions despite its +5 charge. In contrast, progressively higher degrees of peptoid supramolecular structure display progressively greater resistance to salting out, which we attribute to the greater entropic stability associated with the complexation of multimeric peptoid bundles.

INTRODUCTION

Although polyelectrolyte complexes (PECs) for drug-delivery applications have been studied for decades,[2-5] controlling the nature and strength of the non-covalent complexation interactions between a small-molecule macro-ion drug and a polyelectrolyte delivery platform remains an important challenge in a number of emerging applications.[6] In the particular case of antimicrobials and anti-infectives, such complexation-based delivery is an important technological solution [7, 8] and has been demonstrated using polyelectrolyte hydrogels and small-molecule antimicrobials such as vancomycin [9] and gentamycin,[10] among others.

We have been studying complexation-based delivery to create so-called self-defensive surfaces [11, 12] that resist bacterial colonization. Our approach is based on polyanionic microgels with as-synthesized hydrated diameters on the order of 5-50 μm. These can be electrostatically deposited to form a discontinuous sub-monolayer coating on a solid surface. In a subsequent self-assembly step driven by complexation interactions, the surface-attached microgels can be loaded with cationic antimicrobials.[11-13] We have shown that, under certain conditions, the antimicrobials can remain complexed within the microgels for extended periods in buffers or in culture media such as DMEM but their release can nevertheless be triggered when contacted by a bacterium in a process known as contact transfer.[11, 12]

Antimicrobial loading by complexation is relatively straightforward. It can be achieved even in systems that are only weakly interacting - e.g., low electrostatic charge density - by loading from solutions of antimicrobial in buffer with low ionic strength. For instance, colistin - an FDA approved antibiotic with +5 charge at physiological pH - can be rapidly loaded from low-ionic-strength 0.01 M phosphate buffer (pH 7.4; $[Na^+]$ = 0.016 M) in microgels of poly(acrylic acid) (PAA), and it can remain loaded when exposed to colistin-free 0.01 M phosphate buffer for as long as a month or more.[11] However, immersion in colistin-free buffer with higher ionic strength leads to very rapid release because the added salt ions shield the electrostatic complexation interactions, and the unbound colistin molecules can then rapidly diffuse out of their host microgels. Colistin is rapidly released, for example, when colistin-loaded PAA microgels are exposed to phosphate buffered saline (PBS, $[Na^+]$ = 0.14 M). Similarly, vancomycin - another FDA-approved antibiotic with one positive charge - is released when vancomycin-loaded PAA microgels are exposed to vancomycin-free 0.01 M buffer. An *in vivo* drug-delivery application often imposes the constraint that the strength of complexation must withstand the physiological conditions of pH 7.4 and an ionic strength of at least 0.14 M. Hence, understanding what properties of the microgel, the antimicrobial, or both influence the complexation strength is an important foundational challenge.

We have recently demonstrated that aromaticity enhances complexation strength.[14, 15] Introducing aromaticity into the antibiotic by switching from colistin (also known as polymyxin E) to its aromatic relative polymyxin B increases the complexation strength with PAA. Likewise, switching the microgel from PAA to the aromatic poly(styrene sulfonate) (PSS) similarly increases the complexation strength with colistin, an effect we attribute to both the steric effects associated with the pendent aromatic group and to the additional hydrophobic and π interactions.

Here we explore another factor that may enhance complexation strength, namely, the supramolecular structure associated with the antimicrobial. We focus on the complexation between

PAA microgels and a series of cationic low molecular weight (< 2000 Da) peptoids. These peptoids - poly(N-substituted glycine) - are peptide mimics where the functional side chains are attached to the main-chain nitrogen rather than to the α-carbon.[16-18] Peptoids with 13 or fewer monomers and with certain sequences form stable secondary helical structures.[19] Since the hydrogen bonding coming from the peptoid backbone is restricted, chain flexibility is increased, [20] and self-assembly can be promoted by intramolecular hydrophobic interactions from lipophilic side chains or the π-π stacking between aromatic side chains.[16, 21] A number of peptoids have exhibited outstanding performance against bacterial pathogens, [1, 22, 23] viruses,[24] and biofilms.[25]

MATERIALS AND METHODS

Experimental methods

General peptoid synthesis: Reaction steps were performed either on an automated Symphony® X peptide synthesizer (Gyros Protein Technologies, Tuscon, AZ) for TM1, TM6, and TM22 or manually in fritted 10 mL syringes for TM4 under smooth mixing on a VWR® Tube Rocker at 21°C using the sub-monomer method. Rink amide MBHA resin (Gyros Protein Technologies, 0.64 mmol/g) was used as a solid support. Acetylation steps were carried out for 30 min and substitution for 1 h. Acetylation using bromoacetic acid and substitution by various amines was repeated until the desired chain length was achieved. The single oligomers were cleaved and deprotected simultaneously using a cocktail of trifluoroacetic acid/triisopropylsilane/water (95:2.5:2.5 (v/v)) for 30 min. After purification, exchange of the counterion was carried out using a 10 mM solution of aqueous HCl. Lyophilization yielded the desired compound.

Peptoid characterization and purification: Product formation and purity (determined to exceed 95%) were determined by analytical UPLC/MS using a Water Acquity UPLC system equipped with an Acquity Diode Array UV detector and a Waters SQD2 mass spectrometer As the stationary phase, a Waters Acquity UPLC Peptide BEH C18 Column (300 Å pore size, 1.7 µm particle size, 2.1 mm × 100 mm) with an Acquity UPLC BEH C18 VanGuard pre-column (1.7 µm, 2.1 mm × 5 mm) was employed. Elution was performed using an aqueous acetonitrile gradient with 0.1% (*v*/*v*) trifluoroacetic acid added (5–95% acetonitrile (*v*/*v*) over 6.80 min, flow rate: 0.8 mL/min, column temperature: 60 °C). Purification by means of preparative HPLC was carried out using a Waters Prep150LC system equipped with a Waters 2489 UV/Visible detector and a Waters Fraction Collector III collector. As the stationary phase, a Waters XBridge BEH300 Prep C18 column (5 µm particle size, 19 mm × 100 mm) with a Waters XBridge Peptide BEH300 C18 guard column (5 µm particle size, 19 mm × 10 mm) was employed. Elution was performed using an aqueous acetonitrile gradient with 0.1% (*v*/*v*) trifluoroacetic acid added (20–60% acetonitrile (*v*/*v*) over 30 min at a flow rate of 17 mL/min).

Microgel synthesis: PAA microgels were synthesized by thermally initiated membrane emulsification. A precursor solution was prepared from 1.0 ml acrylic acid (Sigma), 0.47 g sodium hydroxide (NaOH, Sigma), 4 ml deionized (DI) water (Millipore type 1), 100 mg ammonium phosphate sulfate (APS, Sigma) and 100 µl poly(ethylene glycol) diacrylate (PEGDA, M_n = 575 Da). Using pressurized nitrogen gas, this precursor solution was forced through a ceramic membrane (1.5 µm pore size (Shirasu Porous Glass (SPG)) into a stirred oil phase (2.56 g Span 80 and 160 ml paraffin oil). The resulting emulsion was deoxygenated (30 min of N_2 bubbling). It

was then heated to 70 °C, held there for 4 h under continuous stirring (500 rpm), and finally allowed to cool. The oil phase was removed by centrifugation and re-suspension in cyclohexane (2x), then in ethanol (10x), and finally in DI water (10x). The resulting microgels in DI water were stored at 4 °C until used for deposition and loading.

In situ microgel loading and assessment of complexation strength. We assessed the complexation strength between PAA microgels and each of four cationic peptoids by following microgel diameter changes *in situ* during peptoid loading from low-ionic strength buffer and then during subsequent exposure to peptoid-free buffer with progressively increasing ionic strength. The four cationic peptoids studied here are referred to as TM1, TM4, TM6, and T22 and are described in detail below (see Fig. 1). The peptoid loading and release experiments followed a procedure we and others have used previously.[11, 14, 22] Briefly, a PDMS gasket with 9 identical holes (3 mm diameter) was bonded to a glass microscope slide to form an array of 9 reaction chambers each with a volume of about 100 μL. Within each chamber, the glass surface was primed with poly(allylamine hydrochloride) (PAH), and PAA microgels were electrostatically deposited onto this primed surface from a colloidal microgel solution (0.01 M phosphate buffer at pH 7.4). The microgel-modified surfaces were washed several times and then equilibrated in 0.01 M buffer at time t = 0. They were then exposed to buffers with dissolved peptoid (loading) and then to peptoid-free buffers with various concentrations of NaCl. We used an inverted optical microscope to record time-resolved digital images, and we normalized the individual microgel diameter during peptoid loading and release to its diameter at time t = 0 (Fig. S1). Adhesion of the microgels to the underlying PAH-primed surface was sufficiently strong that the microgels remained adhered during all loading and release experiments, and we were able to follow specific microgels throughout these processes.

Computational methods

The self-assembly of TM1, TM4, TM6, and T22 was studied using all-atom molecular dynamics (MD) simulations. The atomistic structures and force field parameters for the peptoids were constructed using CHARMM-GUI's ligand reader and modeler function.[26] The simulation box for the MD simulations was created using CHARMM-GUI's solution builder function.[26]

An individual peptoid molecule was solvated in 150 mM NaCl solution for energy minimization and equilibration. Water was modeled using TIP3P,[27] and CHARMM36m[28] parameters were used to model the peptoid. The solvated peptoid was energy minimized using the steepest descent algorithm with a maximum force of 1000 kJ mol^{-1} nm^{-1} and equilibrated in isothermal-isochoric (NVT) and isothermal-isobaric (NPT) ensemble conditions for 2 ns each using GROMACS 2019.[29] The heavy atoms of the peptoids were position restrained during the NVT and NPT runs. The electrostatic and van der Waals interaction cutoff was 1.2 nm, and the time step was set to 2 fs. Production MD runs were performed for 10 ns, where all position constraints were lifted. The particle-mesh Ewald (PME) approach[30] was used to calculate long-range electrostatic interactions. The v-rescale thermostat[31] with temperature coupling constant τ_t = 1.0 ps was employed to keep the temperature constant at 300 K. The Berendsen barostat[32] with a compressibility constant of τ_p = 5.0 ps and a compressibility constant of 4.5×10^{-5} bar^{-1} was used to maintain an isotropic pressure of 1 bar for the NPT run. The nonbonded interaction neighbor list was then updated every 20 steps.

A 20-peptoid system was created for each TM to compare their self-assembly properties. The 20 peptoids were randomly placed in a 12 nm cubic box, charge neutralized by chloride counterions, and solvated with 150 mM NaCl solution. The peptoids and ions were modeled using the CHARMM36m parameters, and water was modeled using TIP3P parameters. Each system was energy minimized using the steepest descent algorithm with 1000 kJ mol^{-1} nm^{-1} maximum force tolerance, followed by NVT and NPT runs for 10 ns each. The heavy atoms of the peptoids were position restrained during these equilibration runs. After equilibration, 1 μs production MD simulations were performed in NPT conditions where all position restraints from the system were removed. The timestep, thermostat, barostat, and coupling constants were the same as in the single peptoid systems described above. An in-house Python script was developed for cluster analysis that utilizes several packages, including MDAnalysis[33] and DBSCAN[34]. A 3 Å cutoff between non-hydrogen atoms of neighboring peptoids was used to define a contact. The peptoid coordinates were extracted from MD production run trajectories at 100 ns intervals for cluster analysis.

RESULTS AND DISCUSSION

The primary structures of the four peptoids - TM1, TM4, TM6, and TM22 - are given in Fig. 1. TM1, TM4, and TM6 are all variations based on a repeated N_{lys}-N_{spe}-N_{spe} motif where N_{lys} is a cationic peptoid mimic of the lysine amino-acid residue and N_{spe} is an α-chiral aromatic. This sequence gives rise to a secondary helical structure with a pitch of 7.0 - 7.6 Å.[35]

TM1 repeats the N_{lys}-N_{spe}-N_{spe} four times.[35] Together with the secondary amine at the N terminus, TM1 has +5 charge at neutral pH. The helicity aligns this charge along one face with the aromatic moieties stacked by π-π coupling to create a hydrophobic face. TM6 is an 11 mer version of TM1 with one N_{spe} unit missing from the C-terminus and likely is helical like TM1.[1] While it is one unit shorter, like TM1, TM6 has a charge of +5 at physiological pH. TM4 is shorter still with only two N_{lys}-N_{spe}-N_{spe} repeats and thus has +3 charge.[36] The 6 mer TM4 furthermore has a para-benzyl bromine substitution on each N_{spe} unit. Due to its shorter length, TM4 is not expected to be helical in structure, but it can self-assemble, likely due to hydrophobic interactions between the bromine atoms and N_{spe} residues. In contrast, TM22 does not form a helix but instead adopts an extended chain conformation. TM22 is structurally and electrostatically similar (+5) to TM1 except that an aliphatic N_{ssb} residue (TM22) substitutes for each N_{spe} residue (TM1). TM22 thus lacks the periodic aromaticity and π-π stacking that drives helix formation in TM1 and TM6.[37, 38]

SAXS indicates that peptoids self-assemble into dimers, trimers, and tetramers

Helicity is important for constructing supramolecular tertiary structures driven by interactions between the hydrophobic regions of amphipathic helices.[39] Small-angle X-ray scattering (SAXS) studies[1] have shown that TM1, TM4, and TM6 monomers self-assemble into combinations of dimer, trimer, and tetramer bundles (Fig. 1, right column and Supporting Information Fig. S2). In solution, approximately 25% of the TM1 is in the form of monomers (individual helices), 50% in the form of dimers (two bundled helices), and the remaining 25% in the form of trimers and tetramers. These previous SAXS experiments showed that solutions of TM6 comprise 60% dimers and 40% monomers. TM4 is almost exclusively in the tetrameric form, which may be due to the strong hydrophobic interaction between Br-substituted aromatic groups.

In the absence of a helical secondary structure, TM22 does not form a supramolecular structure as confirmed by SAXS data (Fig. S2), where the scattering curve can be analyzed using a Gaussian chain model.

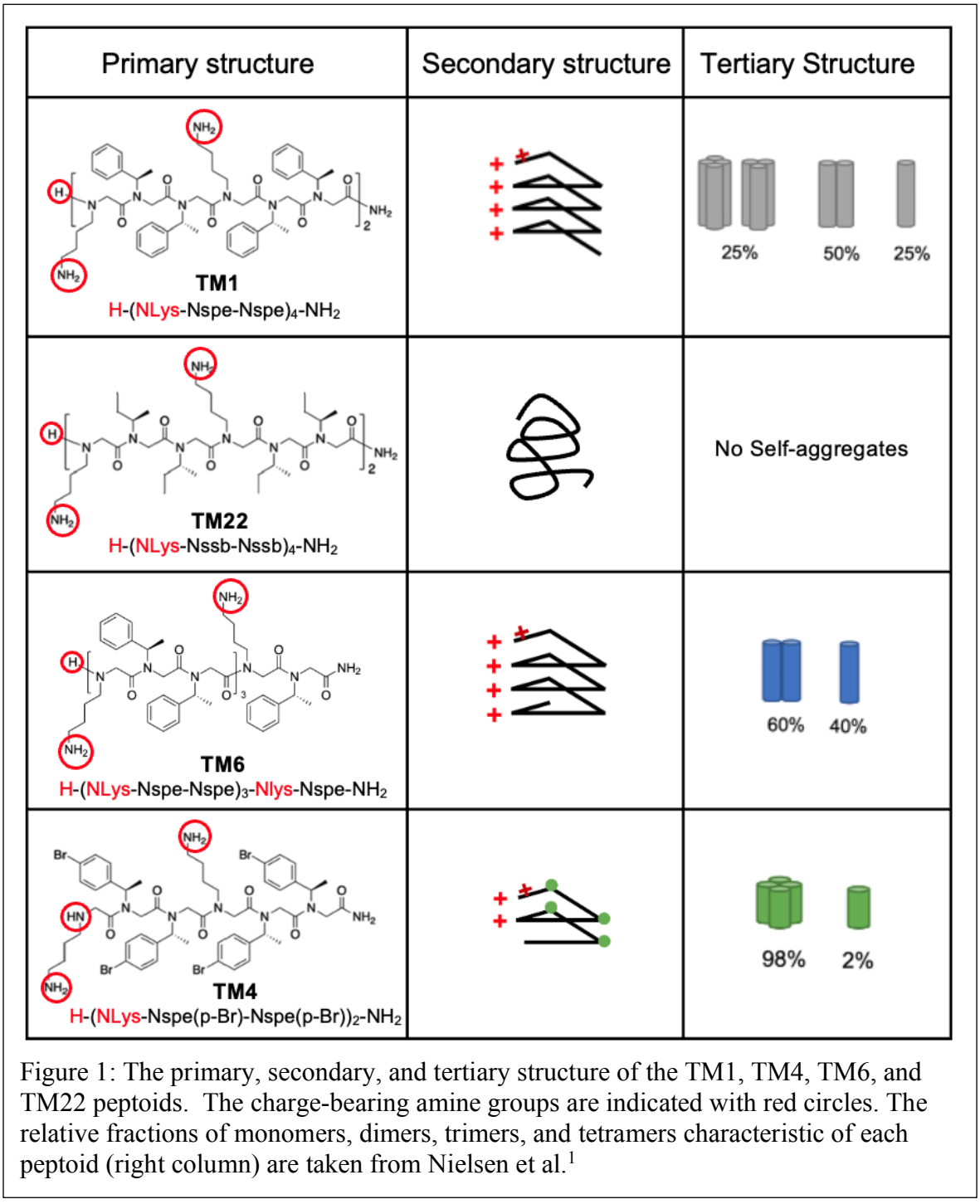

Figure 1: The primary, secondary, and tertiary structure of the TM1, TM4, TM6, and TM22 peptoids. The charge-bearing amine groups are indicated with red circles. The relative fractions of monomers, dimers, trimers, and tetramers characteristic of each peptoid (right column) are taken from Nielsen et al.[1]

Computational self-assembly data are consistent with SAXS results

The assembly of the peptoids into dimers, trimers, tetramers, and larger bundles was computed using well-equilibrated atomistic simulations. The distributions of assembled structures are listed in Table 1. The final (1 μs) snapshots of the simulations are provided in Figure 2.

Table 1. Percent distribution of peptoid clusters predicted by all-atom self-assembly simulations.

	TM1	TM4	TM6	TM22
Monomer	35 ± 10	9 ± 3	50 ± 14	85 ± 11
Dimer	17 ± 13	2 ± 4	23 ± 17	12 ± 11
Trimer	14 ± 13	2 ± 4	11 ± 15	2 ± 4
Tetramer	11 ± 13	2 ± 7	5 ± 8	1 ± 5
Multimer	23 ± 21	85 ± 7	10 ± 19	0

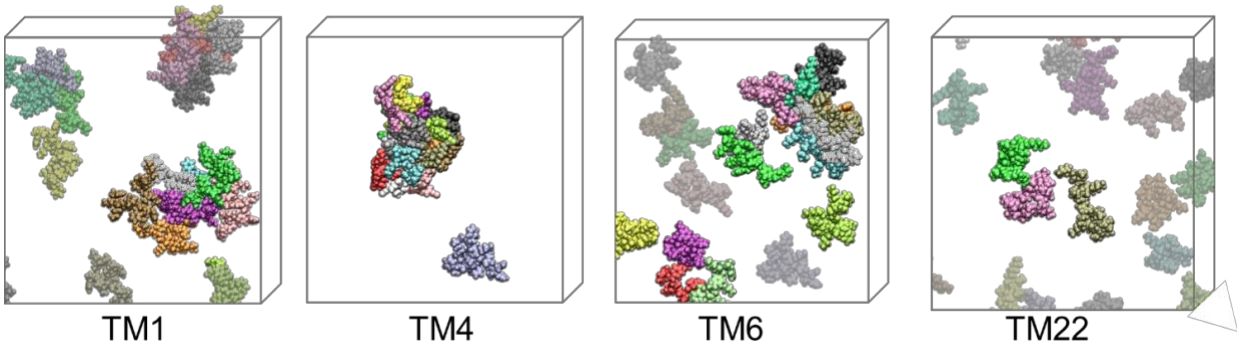

Figure 2. Snapshots of the self-assembled peptoids after 1μs of molecular dynamics simulations. Each system contains 20 molecules of peptoids (individually colored). Water and counterions are omitted for clarity.

We find that 35 ± 10% of the TM1 peptoids are in the form of a monomer. The rest appear as dimers, trimers, tetramers, and higher order bundles (multimers). In contrast, TM22 does not self-assemble. The majority of the TM22 peptoids are monomers (85 ± 11%), with a small percentage of short-lived dimers (12%) and trimers (2%). This is consistent with the SAXS data. The TM6 self-assembly distribution indicates 50 ± 14% in monomeric form, 23 ± 17% as dimers, and 11 ± 15% as trimers. The high-standard deviations show that the clustering of TM6 is dynamic, and the instantaneous distribution values are close to those measured experimentally.

In the case of TM4, the simulations show the formation of large aggregates with only 9 ± 3% of the peptoids as monomers. While the simulations and the SAXS measurements agree that there is a very low monomer concentration, the experiments indicate that the remaining TM4 (98%)

is in tetramer form whereas the simulations indicate the formation of higher order multimer bundles (Fig. 2).

To examine the role of hydrophobicity in the self-assembly of peptoids into higher-order bundles, we computed the hydropathy of the Nlys, Nspe, Nssh, and Br-substituted Nspe building blocks using the Protocol for Assigning a Residue's Character on the Hydropathy (PARCH) scale.[40] Figure 3 shows that parch values of each residue in TM1, TM22, TM6, and TM4 peptoids. Low parch values indicate hydrophobic behavior. Among the four peptoids, TM4 is the most hydrophobic peptoid with all parch values in the 0.1 - 0.4 range, which is consistent with the finding that TM4 exhibits the highest degree of self-assembly into clusters. In contrast, TM22 has multiple residues with parch values in the 0.5-0.8 range. TM1 also has residues with high parch values in the 0.5 - 1.2 range. However, TM1 assembles, whereas TM22 does not because TM22 lacks aromatic rings. Like TM1, TM6 also assembles due to the presence of aromaticity, but its assembly is slightly lower than TM1 because it is a shorter peptoid with one less aromatic ring. The self-assembly simulations and the parch scale calculations show that the hydrophobicity of the residues and the presence of aromatic rings promote peptoid assembly into higher-order multimeric bundles.

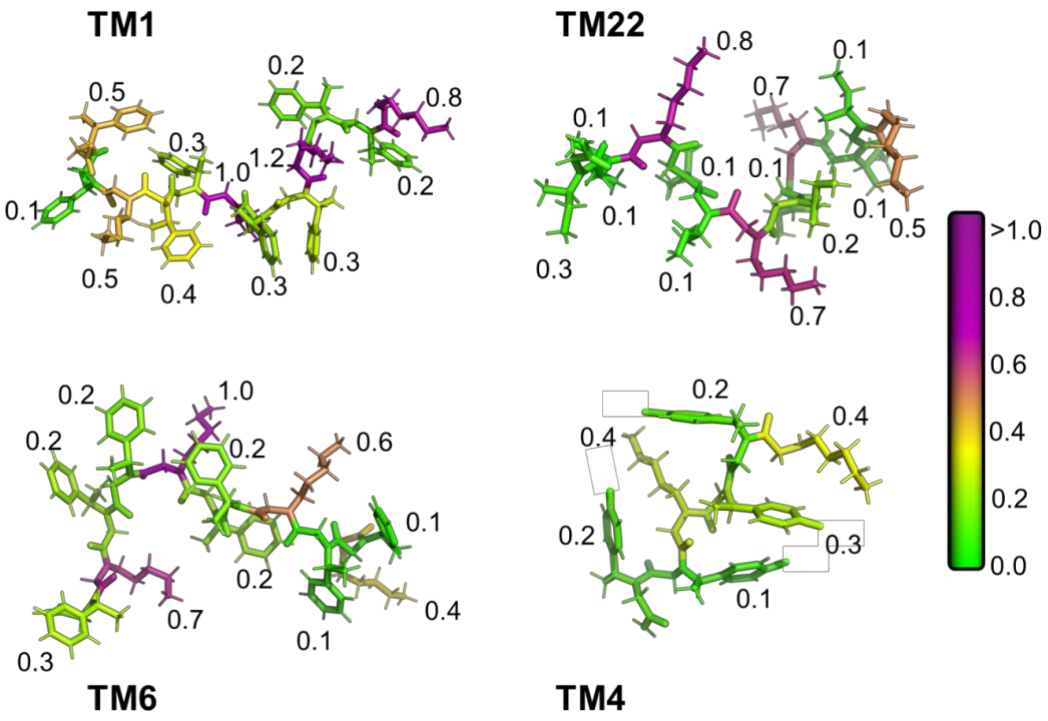

Figure 3. Hydropathy of the TM1, TM22, TM6, and TM4 peptoids. The residues are colored based on the parch values on the color scale (right), where green and purple colors indicate hydrophobic and hydrophilic residues, respectively.

Experiments show that supramolecular structure increases complexation strength.

Figure 4 follows the average diameter change during loading from solutions of 1 mg/mL peptoid dissolved in 0.01 M phosphate buffer. During complexation loading, the microgel diameters decrease asymptotically until they reach a final diameter beyond which the diameter does not change. This behavior is very consistent with similar complexation-loading experiments by us and others.[11, 13-15, 41-44] The microgel diameters decrease for at least two reasons. First, for each complexation event between a PAA acid group and a peptoid amine group, a Na^+ counterion is released to the surrounding buffer thus reducing the osmotic pressure responsible for the swelling of the unloaded gel. Second, since the peptoids are multivalent, complexation introduces an additional set of crosslinks that reduces the average gel mesh size. The fact that the microgel diameter decreases (Fig. 4) indicates loading. The loading of TM22 is complete within three minutes. We note that deswelling occurs under the mechanical constraint that the contact between the gel and the PAH-primed substrate does not change. The fact that TM22 loading produces a spherical microgel morphology suggests uniform loading. The other three peptoids load more slowly, and their loaded morphologies are more complex. The wrinkled morphology characteristic of TM1 and TM4 loading suggests that a buckling instability occurs to relieve stresses that arise during deswelling. TM6 loading avoids wrinkling, but the speckled dark contrast within the loaded microgels suggests that there may be some degree of phase separation. Diameter measurements were made using the central part of each image where there is a strong and rotationally symmetric change in contrast. The average as-loaded diameters (n = 50) normalized to the initial unloaded diameters (LND) were: LND_{TM1} = 36% ± 3%; LND_{TM22} = 39% ± 2%; LND_{TM6} = 45%±4%; and LND_{TM4} = 40%±4%. Previous measurements[22] of the loading amount and zeta potential indicate that TM1 loading completely neutralizes the PAA charge indicating that the microgel is fully loaded.

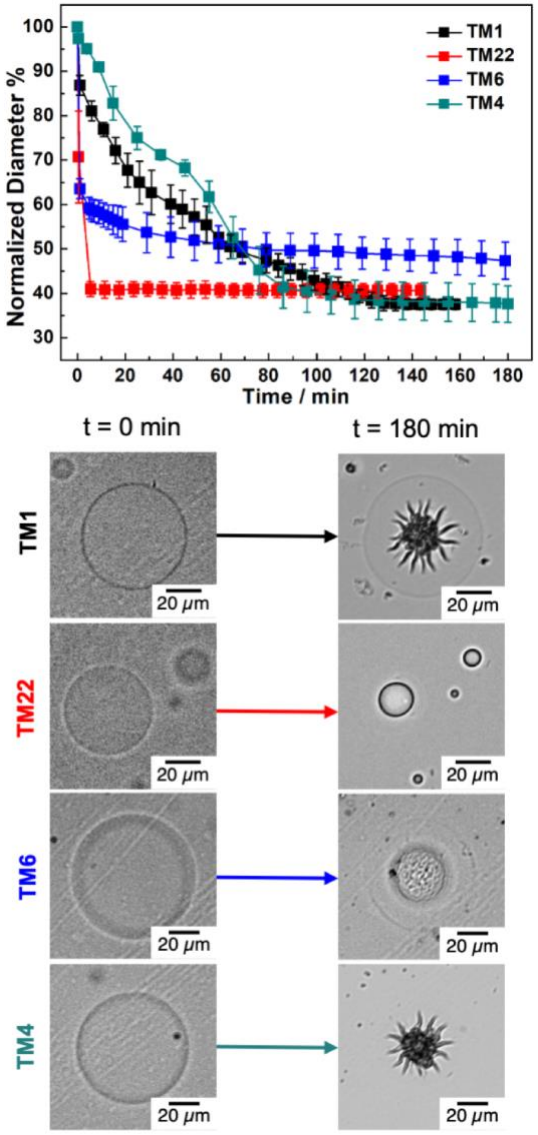

Figure 4. *In-situ* peptoid loading. (Top) Time-resolved change in microgel diameter indicates peptoid loading (1 mg/ml peptoid in 0.01 M phosphate buffer) by complexation with PAA microgels (n = 5). (Bottom) Bright-field optical microscope images of PAA microgels before loading (t = 0 min) and completely loaded (t = 180 min).

To assess the relative complexation strengths, the loaded microgels were exposed to peptoid-free phosphate buffer with a well-defined [Na^+], and the time-resolved microgel diameters were measured for soaking periods of 960 min. At the end of this soaking period, the soaking buffer was replaced with 0.01 M phosphate buffer. This final step enabled us to isolate diameter changes due to peptoid decomplexation from those due to the different ionic strengths of the buffer.[14] Fig. 5a illustrates the results of one such set of experiments using TM1-loaded microgels. There is no diameter change when [Na^+] = 0.216 M. This level of complexation stability has enabled us to separately assess both the antimicrobial properties and cytocompatibility of surfaces modified by TM1 loaded PAA microgels under physiologically relevant conditions.[22] Indeed, significant swelling does not occur until [Na^+] = 0.616 M. The fact that this swelling is due to TM1 release is manifested by the diameter increase that occurs when the sample is subsequently equilibrated in 0.01 M buffer (t = 1030 min) at the end of the soaking period. We have observed similar release behavior in other microgel/macro-ion systems.[11, 14] Figure S3 provides additional image data indicating that the microgel diameter increase corresponds to peptoid release. Figure 5a indicates that complete TM1 release occurs after soaking for 800 mins in buffer with [Na^+] = 1.016 M, as manifested by the fact that the average microgel diameter returns to 100% in 0.01 M phosphate buffer.

Measurements similar to those in Fig. 5a were made using microgels loaded with each of the four peptoids and exposed to phosphate buffer with a range of different [Na^+]. In each case, after the soaking period we determined the final normalized diameter, FND, in 0.01 M phosphate buffer. Following Schlenoff et al. [45-47] and our own prior work on colistin complexation with PAA and PSS,[14] we used the LND (loaded normalized diameter) and the FND values to estimate the doping level, y, which measures the fraction of PAA acid sites whose charge is compensated for by a Na^+ rather than by a peptoid amine group:

$$y = \frac{FND^3 - LND^3}{100^3 - LND^3} \qquad \text{...[1]}$$

Full peptoid loading corresponds to y=0, and full release corresponds to y=1.

The doping dependence on ionic strength for each of the four peptoid-microgel complexes is illustrated by Fig. 5b, and there are striking differences. The doping behavior of TM22 indicates relatively weak complexation with PAA. TM22 is fully released when exposed to TM22-free 0.01 M buffer. In contrast, the release of TM1 and TM6 requires significantly higher [Na^+] and is not fully completed until [Na^+] = 1.016 M and 0.466 M, respectively. TM4 exhibits the greatest complexation strength with no release until [Na^+] = 1.016 M.

We recognize that eq. [1] only approximates the doping behavior, because the microgel deswelling and reswelling is constrained by the microgel contact with the substrate (Fig. 4). However, representing the microgel changes based on a different diameter dependence (e.g., linear or quadratic rather than cubic) does not change the trends or relative positions of the doping curves in Fig. 5b. What is significant is the fact that the stability of the microgel-peptoid complex increases as the degree of peptoid supramolecular structure increases.

Comparing TM1 and TM22 is particularly interesting, since their monomeric structures are very similar. The primary difference between them is the presence or absence of aromatic side chains that lead to substantially different tertiary structures. Notably, TM1 comprises dimeric, trimeric, and tetrameric structures while TM22 comprises only monomeric oligomers. The higher order structure effectively concentrates more cationic charge. This has at least two effects. First, a TM1 tetramer, for example, would carry 20+ charge, and equivalently compensating the corresponding PAA acid groups by TM22 would require four monomers. Hence, on a per unit basis, loading a TM1 tetramer will release four times as many counterions than loading a single TM22 monomer. There is thus a higher entropic gain with tetramer complexation. Second, once fully complexed, subsequent release of a tetramer would require 20 acid-amine pairings to be broken simultaneously while release of a monomer would require only 5 such pairings to simultaneously be broken. In the absence of complete compensation by added salt, partial compensation allows local reorganization of the complexed polymer mesh and peptoid, but the long-range range translational diffusion from the inside of a microgel to the surrounding medium remains very restricted.[14]

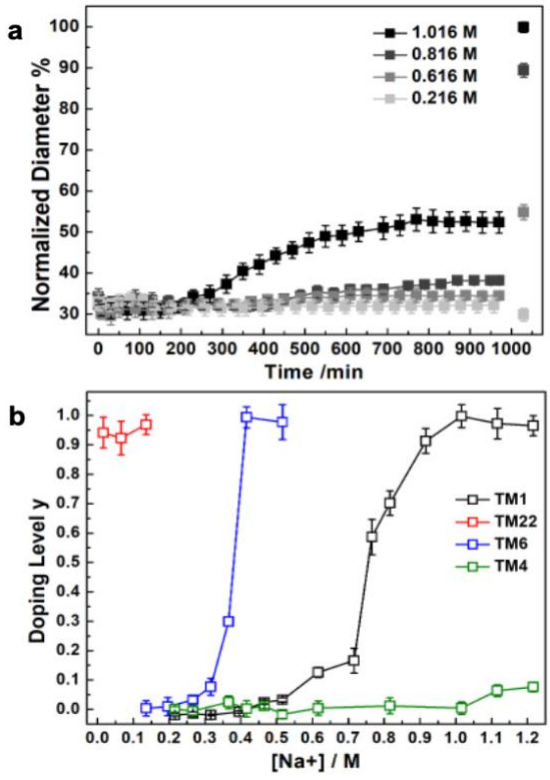

Figure 5. (a) Real-time measurements of microgel diameter follow the complexation of TM1 within PAA microgels when exposed to 0.01 M phosphate buffers with varying [Na^+]. (b) Doping level (y) as a function of [Na^+] in 0.01 M phosphate buffer (n = 5).

In the case of TM1 where the SAXS studies indicate that monomers, dimers, trimers, and tetramers are all present, our *in situ* diameter measurements do not resolve which of these four structures are involved in the initial loading event. If all are present, one might expect to see plateaus in the doping plots of Fig. 5, where each plateau would represent an increment of [Na^+] required to release the next order of supramolecular structure. The fact that we do not see such plateaus raises the possibility that the higher-order structures preferentially participate in the loading process. Importantly, however, the fact that TM4, which is almost exclusively in tetrameric form, remains stably complexed until very high salt concentrations is an indication that it remains it its tetrameric form once complexed. If not, given that the TM4 monomer is only +3 charge, we would expect that it would achieve completed doping and the consequent TM4 release at much lower [Na^+].

CONCLUSIONS

We have found that supramolecular structure increases the complexation strength between a polyanionic microgel and oligomeric cationic peptoids. From a practical point of view, several specific peptoids - TM1, TM6, and TM4 - remain stably complexed at ionic strengths that exceed

0.14 M and, hence, may lend themselves well to triggered drug-delivery applications under physiologically relevant conditions. More broadly, these results suggest that charged macro-ions that assemble into supramolecular structures - e.g., bundles or micelles - will exhibit stronger complexation than their monomeric counterparts, and these supramolecular systems may be more appropriate for *in vivo* antimicrobial applications.

SUPPORTING INFORMATION

In situ optical microscopy configuration. SAXS data. Image data.

ACKNOWLEDGEMENTS

The Stevens and Syracuse portions of this project were supported by an NSF Growing Convergence Research GCR Grant (NSF # 2219014). Computational resources were provided by the Research Computing and Information and Technology Services at Syracuse University. AEB, KBS and JSL thank the NIH for funding through the Director's Pioneer Award (1DP1 OD029517). AEB also acknowledges funding from Stanford University's Discovery Innovation Fund, the Cisco University Research Program Fund, the Silicon Valley Community Foundation, and James J. Truchard and the Truchard Foundation. JEN thanks the Novo Nordisk Foundation, and the Stanford Bio-X Program (NNF21OC0068675) for funding. SAXS data were collected at beamline 12.3.1 at the Advanced Light Source (ALS), a national user facility operated by Lawrence Berkeley National Laboratory on behalf of the DOE Office of Basic Energy Sciences, through the Integrated Diffraction Analysis Technologies (IDAT) program, supported by DOE Office of Biological and Environmental Research. Additional support comes from the NIH project ALS-ENABLE (P30 GM124169) and a High-End Instrumentation grant S10OD018483. We thank Dr. Gregory Hura at the ALS for SAXS support. Work at the Molecular Foundry was supported by the DOE Office of Basic Energy Sciences (contract # DE-AC02-05CH11231). We gratefully acknowledge Drs. Michael Connolly and Natalia Molchanova at the Molecular Foundry for assistance with peptoid synthesis and sample preparation.

REFERENCES

(1) Nielsen, J. E.; Alford, M. A.; Yung, D. B. Y.; Molchanova, N.; Fortkort, J. A.; Lin, J. S.; Diamond, G.; Hancock, R. E. W.; Jenssen, H.; Pletzer, D.; et al. Self-Assembly of Antimicrobial Peptoids Impacts Their Biological Effects on ESKAPE Bacterial Pathogens. *ACS Infect Dis* **2022**, *8* (3), 533-545. DOI: 10.1021/acsinfecdis.1c00536

(2) Lankalapalli, S.; Kolapalli, V. R. Polyelectrolyte Complexes: A Review of their Applicability in Drug Delivery Technology. *Indian J Pharm Sci* **2009**, *71* (5), 481-487. DOI: 10.4103/0250-474x.58165

(3) Jagtap, P.; Patil, K.; Dhatrak, P. Polyelectrolyte complex for drug delivery in biomedical applications: A Review. In *IOP Conference Series: Materials Science and Engineering*, 2021; IOP Publishing: Vol. 1183, p 012007.

(4) Gao, S.; Holkar, A.; Srivastava, S. Protein-Polyelectrolyte Complexes and Micellar Assemblies. *Polymers (Basel)* **2019**, *11* (7), 1097. DOI: 10.3390/polym11071097

(5) Kurinomaru, T.; Shiraki, K. Aggregative protein-polyelectrolyte complex for high-concentration formulation of protein drugs. *Int J Biol Macromol* **2017**, *100*, 11-17. DOI: 10.1016/j.ijbiomac.2016.06.016

(6) Muthukumar, M. 50th Anniversary Perspective: A Perspective on Polyelectrolyte Solutions. *Macromolecules* **2017**, *50* (24), 9528-9560. DOI: 10.1021/acs.macromol.7b01929

(7) Veiga, A. S.; Schneider, J. P. Antimicrobial hydrogels for the treatment of infection. *Biopolymers* **2013**, *100* (6), 637-644. DOI: 10.1002/bip.22412

(8) Du, A. W.; Stenzel, M. H. Drug carriers for the delivery of therapeutic peptides. *Biomacromolecules* **2014**, *15* (4), 1097-1114. DOI: 10.1021/bm500169p

(9) Gustafson, C. T.; Boakye-Agyeman, F.; Brinkman, C. L.; Reid, J. M.; Patel, R.; Bajzer, Z.; Dadsetan, M.; Yaszemski, M. J. Controlled Delivery of Vancomycin via Charged Hydrogels. *PLoS One* **2016**, *11* (1), e0146401. DOI: 10.1371/journal.pone.0146401

(10) Li, H.; Yang, J.; Hu, X.; Liang, J.; Fan, Y.; Zhang, X. Superabsorbent polysaccharide hydrogels based on pullulan derivate as antibacterial release wound dressing. *J Biomed Mater Res A* **2011**, *98* (1), 31-39. DOI: 10.1002/jbm.a.33045

(11) Liang, J.; Wang, H.; Libera, M. Biomaterial surfaces self-defensive against bacteria by contact transfer of antimicrobials. *Biomaterials* **2019**, *204*, 25-35. DOI: 10.1016/j.biomaterials.2019.03.006

(12) Xiao, X.; Zhao, W.; Liang, J.; Sauer, K.; Libera, M. Self-defensive antimicrobial biomaterial surfaces. *Colloids Surf B Biointerfaces* **2020**, *192*, 110989. DOI: 10.1016/j.colsurfb.2020.110989

(13) Eichenbaum, G. M.; Kiser, P. F.; Simon, S. A.; Needham, D. pH and Ion-Triggered Volume Response of Anionic Hydrogel Microspheres. *Macromolecules* **1998**, *31* (15), 5084-5093. DOI: 10.1021/ma970897t

(14) Xiao, X.; Ji, J.; Zhao, W.; Nangia, S.; Libera, M. Salt Destabilization of Cationic Colistin Complexation within Polyanionic Microgels. *Macromolecules* **2022**, *55* (5), 1736-1746.

(15) Xiao, X.; Ji, J.; Wang, H.; Nangia, S.; Wang, H.; Libera, M. Self-Defensive Antimicrobial Surfaces Using Polymyxin-Loaded Poly(styrene sulfonate) Microgels. *ACS Biomater Sci Eng* **2022**, *8* (11), 4827-4837. DOI: 10.1021/acsbiomaterials.2c00783

(16) Park, M.; Jardetzky, T. S.; Barron, A. E. NMEGylation: a novel modification to enhance the bioavailability of therapeutic peptides. *Biopolymers* **2011**, *96* (5), 688-693. DOI: 10.1002/bip.21607

(17) Chongsiriwatana, N. P.; Patch, J. A.; Czyzewski, A. M.; Dohm, M. T.; Ivankin, A.; Gidalevitz, D.; Zuckermann, R. N.; Barron, A. E. Peptoids that mimic the structure, function, and mechanism of helical antimicrobial peptides. *Proc Natl Acad Sci U S A* **2008**, *105* (8), 2794-2799. DOI: 10.1073/pnas.0708254105

(18) Zuckermann, R. N. Peptoid origins. *Biopolymers* **2011**, *96* (5), 545-555. DOI: 10.1002/bip.21573

(19) Mojsoska, B.; Zuckermann, R. N.; Jenssen, H. Structure-activity relationship study of novel peptoids that mimic the structure of antimicrobial peptides. *Antimicrob Agents Chemother* **2015**, *59* (7), 4112-4120. DOI: 10.1128/aac.00237-15

(20) Castelletto, V.; Seitsonen, J.; Tewari, K. M.; Hasan, A.; Edkins, R. M.; Ruokolainen, J.; Pandey, L. M.; Hamley, I. W.; Lau, K. H. A. Self-Assembly of Minimal Peptoid Sequences. *ACS Macro Lett* **2020**, *9* (4), 494-499. DOI: 10.1021/acsmacrolett.9b01010

(21) Lau, K. H.; Castelletto, V.; Kendall, T.; Sefcik, J.; Hamley, I. W.; Reza, M.; Ruokolainen, J. Self-assembly of ultra-small micelles from amphiphilic lipopeptoids. *Chem Commun (Camb)* **2017**, *53* (13), 2178-2181. DOI: 10.1039/c6cc09888f

(22) Zhao, W.; Wang, H.; Xiao, X.; De Stefano, L.; Katz, J.; Lin, J. S.; Barron, A. E.; Schaer, T. P.; Wang, H.; Libera, M. Peptoid-Loaded Microgels Self-Defensively Inhibit Staphylococcal Colonization of Titanium in a Model of Operating-Room Contamination. *Advanced Materials Interfaces* **2022**, *9* (31), 2201662.

(23) Czyzewski, A. M.; Jenssen, H.; Fjell, C. D.; Waldbrook, M.; Chongsiriwatana, N. P.; Yuen, E.; Hancock, R. E.; Barron, A. E. In Vivo, In Vitro, and In Silico Characterization of Peptoids as Antimicrobial Agents. *PLoS One* **2016**, *11* (2), e0135961. DOI: 10.1371/journal.pone.0135961

(24) Diamond, G.; Molchanova, N.; Herlan, C.; Fortkort, J. A.; Lin, J. S.; Figgins, E.; Bopp, N.; Ryan, L. K.; Chung, D.; Adcock, R. S.; et al. Potent Antiviral Activity against HSV-1 and SARS-CoV-2 by Antimicrobial Peptoids. *Pharmaceuticals (Basel)* **2021**, *14* (4), 304. DOI: 10.3390/ph14040304

(25) Lin, J. S.; Bekale, L. A.; Molchanova, N.; Nielsen, J. E.; Wright, M.; Bacacao, B.; Diamond, G.; Jenssen, H.; Santa Maria, P. L.; Barron, A. E. Anti-persister and Anti-biofilm Activity of Self-Assembled Antimicrobial Peptoid Ellipsoidal Micelles. *ACS Infect Dis* **2022**, *8* (9), 1823-1830. DOI: 10.1021/acsinfecdis.2c00288

(26) Jo, S.; Kim, T.; Iyer, V. G.; Im, W. CHARMM-GUI: A web-based graphical user interface for CHARMM. *Journal of Computational Chemistry* **2008**, *29* (11), 1859-1865. DOI: https://doi.org/10.1002/jcc.20945

(27) Mark, P.; Nilsson, L. Structure and Dynamics of the TIP3P, SPC, and SPC/E Water Models at 298 K. *The Journal of Physical Chemistry A* **2001**, *105* (43), 9954-9960. DOI: 10.1021/jp003020w

(28) Huang, J.; Rauscher, S.; Nawrocki, G.; Ran, T.; Feig, M.; de Groot, B. L.; Grubmüller, H.; MacKerell, A. D. CHARMM36m: an improved force field for folded and intrinsically disordered proteins. *Nature Methods* **2017**, *14* (1), 71-73. DOI: 10.1038/nmeth.4067

(29) Abraham, M. J.; Murtola, T.; Schulz, R.; Páll, S.; Smith, J. C.; Hess, B.; Lindahl, E. GROMACS: High performance molecular simulations through multi-level parallelism from laptops to supercomputers. *SoftwareX* **2015**, *1-2*, 19-25. DOI: https://doi.org/10.1016/j.softx.2015.06.001

(30) Petersen, H. G. Accuracy and efficiency of the particle mesh Ewald method. *The Journal of Chemical Physics* **1995**, *103* (9), 3668-3679. DOI: 10.1063/1.470043.

(31) Bussi, G.; Donadio, D.; Parrinello, M. Canonical sampling through velocity rescaling. *The Journal of Chemical Physics* **2007**, *126* (1), 014101. DOI: 10.1063/1.2408420.

(32) Berendsen, H. J. C.; Postma, J. P. M.; van Gunsteren, W. F.; DiNola, A.; Haak, J. R. Molecular dynamics with coupling to an external bath. *The Journal of Chemical Physics* **1984**, *81* (8), 3684-3690. DOI: 10.1063/1.448118.

(33) Michaud-Agrawal, N.; Denning, E. J.; Woolf, T. B.; Beckstein, O. MDAnalysis: A toolkit for the analysis of molecular dynamics simulations. *Journal of Computational Chemistry* **2011**, *32* (10), 2319-2327. DOI: https://doi.org/10.1002/jcc.21787

(34) Ester, M.; Kriegel, H.-P.; Sander, J.; Xu, X. A density-based algorithm for discovering clusters in large spatial databases with noise. In Proceedings of the Second International Conference on Knowledge Discovery and Data Mining, Portland, Oregon; 1996.

(35) Patch, J. A.; Barron, A. E. Helical peptoid mimics of magainin-2 amide. *J Am Chem Soc* **2003**, *125* (40), 12092-12093. DOI: 10.1021/ja037320d

(36) Molchanova, N.; Nielsen, J. E.; Sørensen, K. B.; Prabhala, B. K.; Hansen, P. R.; Lund, R.; Barron, A. E.; Jenssen, H. Halogenation as a tool to tune antimicrobial activity of peptoids. *Sci Rep* **2020**, *10* (1), 14805. DOI: 10.1038/s41598-020-71771-8

(37) Wu, C. W.; Kirshenbaum, K.; Sanborn, T. J.; Patch, J. A.; Huang, K.; Dill, K. A.; Zuckermann, R. N.; Barron, A. E. Structural and spectroscopic studies of peptoid oligomers with alpha-chiral aliphatic side chains. *J Am Chem Soc* **2003**, *125* (44), 13525-13530. DOI: 10.1021/ja037540r

(38) Wu, C. W.; Sanborn, T. J.; Huang, K.; Zuckermann, R. N.; Barron, A. E. Peptoid oligomers with alpha-chiral, aromatic side chains: sequence requirements for the formation of stable peptoid helices. *J Am Chem Soc* **2001**, *123* (28), 6778-6784. DOI: 10.1021/ja003154n

(39) Woolfson, D. N. The design of coiled-coil structures and assemblies. *Adv Protein Chem* **2005**, *70*, 79-112. DOI: 10.1016/S0065-3233(05)70004-8

(40) Ji, J.; Carpentier, B.; Chakraborty, A.; Nangia, S. An Affordable Topography-Based Protocol for Assigning a Residue's Character on a Hydropathy (PARCH) Scale. *Journal of Chemical Theory and Computation* **2023**, *Article ASAP*. DOI: 10.1021/acs.jctc.3c00106

(41) Al-Tikriti, Y.; Hansson, P. Drug-Induced Phase Separation in Polyelectrolyte Microgels. *Gels* **2022**, *8* (1), 4.

(42) Bysell, H.; Malmsten, M. Visualizing the interaction between poly-L-lysine and poly(acrylic acid) microgels using microscopy techniques: Effect of electrostatics and peptide size. *Langmuir* **2006**, *22* (12), 5476-5484, Article. DOI: 10.1021/la060452a

(43) Eichenbaum, G. M.; Kiser, P. F.; Dobrynin, A. V.; Simon, S. A.; Needham, D. Investigation of the Swelling Response and Loading of Ionic Microgels with Drugs and Proteins: The Dependence on Cross-Link Density. *Macromolecules* **1999**, *32*, 4867-4878.

(44) Johansson, C.; Hansson, P.; Malmsten, M. Interaction between lysozyme and poly(acrylic acid) microgels. *J. Colloid Interface Sci.* **2007**, *316* (2), 350-359, Article. DOI: 10.1016/j.jcis.2007.07.052

(45) Farhat, T. R.; Schlenoff, J. B. Doping-controlled ion diffusion in polyelectrolyte multilayers: mass transport in reluctant exchangers. *J Am Chem Soc* **2003**, *125* (15), 4627-4636. DOI: 10.1021/ja021448y

(46) Fu, J.; Fares, H. M.; Schlenoff, J. B. Ion-pairing strength in polyelectrolyte complexes. *Macromolecules* **2017**, *50* (3), 1066-1074.

(47) Schlenoff, J. B. Site-specific perspective on interactions in polyelectrolyte complexes: Toward quantitative understanding. *J Chem Phys* **2018**, *149* (16), 163314. DOI: 10.1063/1.5035567

Table of Contents graphic